Motion Correction and Attenuation Correction for Respiratory Gated PET Images

Wenjia Bai
wenjia@robots.ox.ac.uk
Sir Michael Brady
jmb@robots.ox.ac.uk

Wolfson Medical Vision Laboratory
University of Oxford
Oxford, UK

Abstract

Positron emission tomography (PET) is a molecular imaging technique which is now widely established as a powerful tool for diagnosing a variety of cancers. However, PET images are substantially degraded by respiratory motion, to the extent that this may adversely impact upon subsequent diagnosis. A motion correction and attenuation correction method is proposed to align the gated PET images and then correct for attenuation. Experimental results show that this method can effectively correct for respiratory motion and improve PET image quality.

1 Introduction

Positron emission tomography (PET) is a molecular imaging technique which is now widely established as a powerful tool for diagnosing a variety of cancers. However, PET images are substantially degraded by respiratory motion to the extent that this may, particularly for thoracic imaging, adversely impact upon subsequent diagnosis. In terms of the magnitude of motion, the diaphragm typically moves about 15-20 mm due to respiration; since current PET scanners have a spatial resolution of approximately 5 mm full width half maximum (FWHM), respiration substantially reduces the effective spatial resolution.

Gated acquisition of PET data has been proposed to overcome the respiratory motion effects. Typically, a respiratory cycle is divided into a number of gates, during each of which the imaged object is assumed to be static. Several different approaches have been proposed to register respiratory gated PET images. Lamare et al. proposed a B-spline deformable algorithm for image registration [4]. Lamare's method relies on dual gating of PET and CT. Gated CT scans can provide accurate deformation fields for motion correction. However, it significantly increases the radiation burden to the patient. Dawood et al. used the optic flow method to estimate motion from PET images without attenuation correction [3]. Therefore, gated CT acquisition is avoided. Attenuation correction of the motion corrected image was mentioned in the discussion section of Dawood's paper, however, does not seem to have been explored. Since attenuation correction is crucial for quantitatively analysing a PET image, it is necessary to further explore the attenuation correction of the motion corrected image.

In this work, we propose a motion correction method for respiratory gated PET images. It is different from previous methods in two aspects. First, motion correction is performed

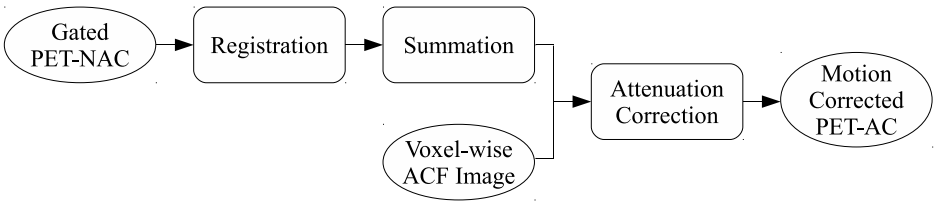

Figure 1: The flowchart for motion correction and attenuation correction.

using a regularised registration algorithm. Second, the motion corrected image is further attenuation corrected using a voxel-wise attenuation correction factor (ACF) image. Experimental results show that this method can effectively correct for respiratory motion and improve PET image quality.

2 Methods

2.1 Framework

Respiratory gating divide PET data into a number of gates, each corresponding to a phase of the respiratory cycle. In this way, the data for each gate contain only slight motion and thus can be regarded as static. Prior to the PET scan, a CT scan is acquired to provide both anatomical information and attenuation correction. Because respiration can be monitored using a respiratory gating device during both PET and CT acquisitions, the CT scan can be matched to a gate of the PET scan.

Because this CT scan matches only one gate and does not align with the other gates, it can not used for attenuation correction of the other gates. Otherwise, artefacts are introduced in reconstruction [3]. Therefore, we reconstruct gated non-attenuation corrected PET (PET-NAC) images and use these PET-NAC images for motion correction. The gate coincident with the CT scan is regarded as the "reference" image, whereas the other gates are regarded as "test" images. The deformation fields between the reference and test images are estimated using B-spline registration [1, 5]. After all the images are aligned to the same position, they are summed to form a motion corrected image.

Because the motion corrected image aligns with the CT scan, it can be accurately attenuation corrected. We generate a voxel-wise ACF image for the reference gate. The ACF image is applied to the motion corrected image, resulting in an attenuation corrected PET (PET-AC) image. The whole framework is illustrated in Figure 1.

2.2 Registration

The goal of registration is to find a transformation $g : x \rightarrow g(x|\theta)$ which maps the reference image $f_r(x)$ to a test image $f_t(x)$ so that $f_r(x)$ corresponds to $f_t(g(x|\theta))$ at each location, $x \in \Omega$ denotes a pixel in a 3-D PET image, and θ denotes the B-spline control points located on a 3-D lattice. The local deformation $g(x|\theta)$ is determined by the weighted sum of its neighbouring control points [5].

Registration is formulated as an optimisation problem, where a cost function consists of a data term which measures the discrepancy between the reference image $f_r(x)$ and the transformed test image $f_t(g(x|\theta))$, and a regularisation term. We use the negative correlation coefficient (CC) to measure the discrepancy of two gated images, since it has the merits of both mathematical simplicity and computational efficiency. The regularisation term is derived, assuming that the control point lattice θ is a Markov random field (MRF), which imposes a local smoothness constraint on the deformation field [1].

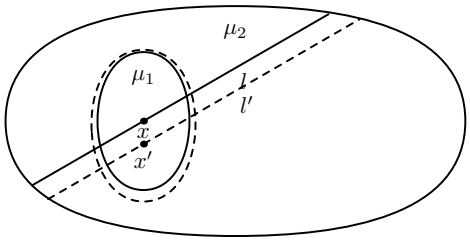

Figure 2: A diagrammatic model of the chest. It mainly consists of two two tissue types of different attenuation coefficients $_1$ and $_2$, representing the lung and the body respectively. l denotes the intersection between a gamma ray and the medium. Due to respiratory motion, the lung deforms (from the solid curve to the dashed curve), the voxel x moves to x', and the intersection l moves to l'.

2.3 Attenuation Correction

Figure 2 shows a diagrammatic model of the chest, which mainly consists of two tissue types of attenuation coefficients $_1$ and $_2$, representing the lung and the body respectively. According to Chang's paper [2], the attenuation at point x can be estimated as,

$$A(x) = \frac{1}{M}\sum_{i=1}^{M} e^{-\ _1 l_{i,1} - \ _2 l_{i,2}} \tag{1}$$

where M denotes the total number of projections. The reciprocal of $A(x)$ can be used for attenuation correction of the intensity of each voxel, and is named the attenuation correction factor (ACF) image. If the model deforms slightly, the change of $A(x)$ can be approximated as,

$$\begin{aligned} dA &= A_t(g(x|\theta)) - A_r(x) \\ &\approx \frac{1}{M}\sum_{i=1}^{M} e^{-\ _1 l_{i,1} - \ _2 l_{i,2}} \cdot (-\ _1 dl_{i,1} - \ _2 dl_{i,2}) \end{aligned} \tag{2}$$

where $A_r(x)$ and $A_t(g(x|\theta))$ denote the attenuation factor of a voxel in the reference image and the test image respectively. In normal respiration, the diaphragm moves 20 mm in maximum. If we select the mid-expiration gate as the reference image, the largest movement between two gates is about 10 mm. Considering the dimension of the chest, the magnitude of the movement is fairly small. The approximation in Equation 2 can be justified by Taylor expansion. It follows that,

$$\begin{aligned} |dA| &\leq \frac{1}{M}\sum_{i=1}^{M} e^{-\ _1 l_{i,1} - \ _2 l_{i,2}} \cdot |\ _1 dl_{i,1} + \ _2 dl_{i,2}| \\ &\leq \frac{1}{M}\sum_{i=1}^{M} e^{-\ _1 l_{i,1} - \ _2 l_{i,2}} \cdot \ _m |dl_{i,m}| \\ &\leq A \cdot \ _m |dl_m| \end{aligned} \tag{3}$$

where $_m = \max(\ _1, \ _2)$, $|dl_{i,m}| = \max(|dl_{i,1}|, |dl_{i,2}|, |dl_i|)$, $|dl_m| = \max_i |dl_{i,m}|$.

The two tissue types represent the lung and the body respectively. We have $_1 = 0.0032 mm^{-1}$ (lung) and $_2 = 0.0096 mm^{-1}$ (body). Therefore, $|dA| \leq A \cdot \ _m dl_m = 0.096A$. As we can see, $|dA|$ is fairly small and negligible. As a result, $A_r(x) \approx A_t(g(x|\theta))$. Because the ACF is the reciprocal of A, we have $ACF_r(x) \approx ACF_t(g(x|\theta))$. It means that we can use the voxel-wise

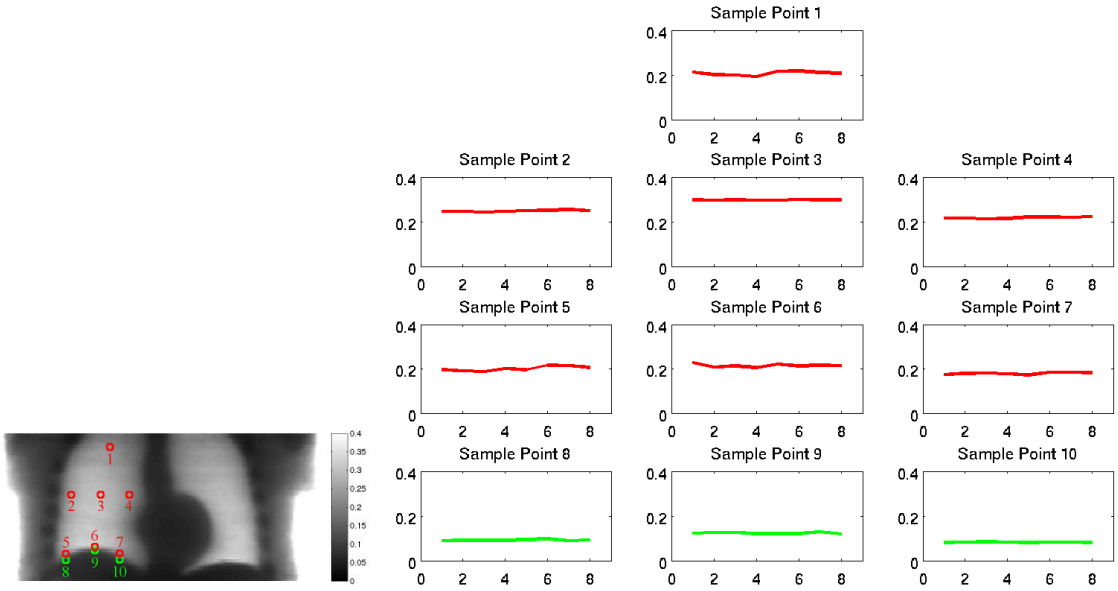

(a) Attenuation image (b) Plot of the attenuation factors against gates

Figure 3: Observation of the changes of attenuation factors for the sample points. The sample points in the right lung are shown in red, whereas those in the liver are shown in green.

ACF image for the reference gate to attenuation correct all the other gates. In practice, the ACF image is generated by reconstructing the reference gate twice, respectively with and without attenuation correction using the CT scan, and then dividing the two reconstructions,

$$ACF_r(x) = \frac{f_{r,AC}(x)}{f_{r,NAC}(x)} \tag{4}$$

After all the PET-NAC images are aligned to the reference gate, they are summed to form a motion-corrected PET-NAC image $f_{sum,NAC}$. This image is then attenuation corrected using the voxel-wise ACF image,

$$f_{sum,AC}(x) = f_{sum,NAC}(x) \cdot ACF_r(x) \tag{5}$$

The whole process can be achieved using any existing reconstruction program. The only additional work is image division and multiplication. It is straightforward to implement.

Table 1: The attenuation factors of the sample points and the changes. A_i denotes the attenuation factor for Gate i, and S_j denotes the jth sample point. The change dA is calculated as the difference between A_i and A_1, where Gate 1 is regarded as the reference gate.

	S_1	S_2	S_3	S_4	S_5	S_6	S_7	S_8	S_9	S_{10}
A_1	0.212	0.247	0.297	0.216	0.196	0.229	0.173	0.089	0.123	0.080
A_2	0.200	0.246	0.296	0.216	0.191	0.207	0.179	0.090	0.126	0.082
A_3	0.199	0.243	0.297	0.213	0.187	0.213	0.181	0.091	0.126	0.085
A_4	0.192	0.246	0.297	0.214	0.201	0.206	0.177	0.090	0.121	0.082
A_5	0.216	0.249	0.297	0.221	0.196	0.221	0.172	0.095	0.120	0.081
A_6	0.218	0.250	0.300	0.220	0.216	0.213	0.183	0.098	0.121	0.083
A_7	0.211	0.254	0.298	0.220	0.215	0.217	0.184	0.090	0.129	0.082
A_8	0.208	0.249	0.298	0.222	0.206	0.214	0.182	0.093	0.119	0.082
$Mean(dA/A_1)$	0.039	0.012	0.003	0.016	0.049	0.068	0.038	0.042	0.025	0.024

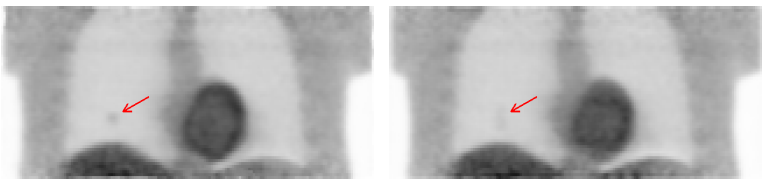

(a) Corrected (b) Uncorrected

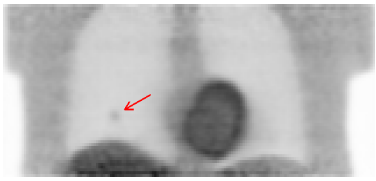

(c) Static

Figure 4: The motion corrected image, the uncorrected image, and the static image. A 10 mm lesion at the bottom of the right lung is annotated by a red arrow.

3 Results

We simulated highly realistic PET data using a Monte-Carlo based PET simulator PET-SORTEO. The human anatomy during respiration was modelled by the NCAT phantom. In order to validate the approximation $A_r(x) \approx A_t(g(x|\theta))$, we observed a number of sample points near the boundaries of the right lung and the liver, where the change of attenuation is most drastic during respiration. The attenuation factors of the sample points are plotted against gates in Figure 3 (b). As we can see from the figure, even at boundary positions, the change of attenuation is relatively small. Table 1 lists the attenuation factors of the sample points and the corresponding changes.

Figure 4 compares the motion corrected image, the uncorrected image, and the static image. The static image is the reconstruction of ideal PET data without any motion, which represents the upper bound of image quality, given the current PET scanner and the reconstruction algorithm used. It is difficult to see the 10 mm lesion in the uncorrected image and it is very likely to be missed by a human observer. However, it can be seen clearly in the motion corrected image and its appearance is similar to that in the static image.

4 Conclusions

The experimental results show that our motion correction method can effectively correct for respiratory motion and improve PET image quality. Attenuation correction is performed using an ACF image and is straightforward to implement.

References

[1] W. Bai and M. Brady. Respiratory motion correction in PET images. *Physics in Medicine and Biology*, 54: 2719–2736, 2009.

[2] L.T. Chang. A method for attenuation correction in radionuclide computed tomography. *IEEE Transactions on Nuclear Science*, 25(1):638–643, 1978.

[3] M. Dawood, F. Buther, X. Jiang, and KP Schafers. Respiratory motion correction in 3-D PET data with advanced optical flow algorithms. *IEEE Transactions on Medical Imaging*, 27(8):1164–1175, 2008.

[4] F. Lamare, M.J. Ledesma Carbayo, T. Cresson, G. Kontaxakis, A. Santos, C. Cheze LeRest, A.J. Reader, and D. Visvikis. List-mode-based reconstruction for respiratory motion correction in PET using non-rigid body transformations. *Physics in Medicine and Biology*, 52:5187–5204, 2007.

[5] P. Thevenaz and M. Unser. Optimization of mutual information for multiresolution image registration. *IEEE Transactions on Image Processing*, 9(12):2083–2099, 2000.